Nanoscale

PAPER

View Article Online
View Journal

Cite this: DOI: 10.1039/c9nr08570j

Exploiting the protein corona: coating of black phosphorus nanosheets enables macrophage polarization *via* calcium influx†

Jianbin Mo, ‡[a] Yun Xu, ‡[b] Xiuxiu Wang,‡[a] Wei Wei *[a,b,c] and Jing Zhao *[a,c]

Received 6th October 2019,
Accepted 2nd December 2019

DOI: 10.1039/c9nr08570j

rsc.li/nanoscale

Black phosphorus nanosheets (BPNSs) have substantially promoted biomedical nanotechnology due to their unique photothermal and chemotherapeutic properties. However, there is still a limited molecular understanding of the effects of bio-nano interfaces on BPNSs and the subsequent impacts on physiological systems. Here, it is shown that black phosphorus–corona complexes (BPCCs) could function as immune modulators to promote the polarization of macrophages. Mechanistically, BPCCs could interact with calmodulin to activate stromal interaction molecule 2 and facilitate Ca^{2+} influx in macrophages, which induced the activation of p38 and NF-κB and polarized M0 macrophages to the M1 phenotype. As a result, BPCC-activated macrophages show greater migration towards cancer cells, 1.3–1.9 times higher cellular cytotoxicity and effective phagocytosis of cancer cells. These findings offer insights into the development of potential and unique applications of corona on BPNSs in nanomedicine.

Introduction

Two-dimensional (2D) nanomaterials bring an opportunity for fundamental studies and biological applications due to their attractive and unique properties. By virtue of their special physical and structural features, black phosphorus nanosheets (BPNSs), a novel 2D layered nanomaterial, have been widely used in nanomedicine such as phototherapy and drug delivery.[1–4] Most nanomaterials are rapidly internalized by the mononuclear cells of the phagocyte system following intravenous administration.[5–7] Jiang and Yu *et al.* elegantly demonstrated that BPNSs can be ingested by macrophages and further induce inflammation *in vivo*.[8] However, our understanding of the effects of BPNSs on the cellular function and phenotype of macrophages is greatly limited. More studies are imperative to better elucidate this very important issue to guide the design and application of BPNSs in the biomedical field.

Bio-nano interfaces occur once nanomaterials come into contact with complex physiological environments, such as blood plasma or the cytoplasm.[9–12] After infiltrating into the physiological environment, the physicochemical properties of the nanomaterial are immediately redefined by adsorption of the biomolecular corona from the biological fluid.[13–16] Increasing evidence indicates that these coronal proteins have diverse biological impacts.[17–22] Chen *et al.* pioneered synchrotron radiation-based techniques to reveal the protective effect of the protein corona against the toxicity of gold nanorods.[23] Dong *et al.* creatively conjugated retinol molecules with nanomaterials to facilitate the formation of corona, endowing the nanosystem with targeting abilities.[24] Specifically, the corona can facilitate unexpected interaction between nanomaterials and cells, including triggering of endothelial cell death or thrombocyte activation, which may not appear between native nanomaterials and cells.[25,26] Such novel interactions further pose surprising influence on the *in vivo* application of nanomaterials. In view of the significance of nanomaterial–corona complexes, further investigations of their *in vivo* fate, behaviour and potential biological impacts are greatly needed.

Here, we characterized the corona protein on the surface of BPNSs by liquid chromatography tandem mass spectrometry (LC-MS/MS). The pivotal protein, myosin, on corona could further interact with calmodulin to activate stromal interaction molecule 2 and facilitate Ca^{2+} influx in macrophages to regulate macrophages in a positive way (Scheme 1). Our results will be helpful to rethink the function of corona on macrophage polarization and will play a guiding role for broad applications of nanomaterials in nanomedicine.

[a]State Key Laboratory of Coordination Chemistry, Chemistry and Biomedicine Innovation Center (ChemBIC), School of Chemistry and Chemical Engineering, Nanjing University, Nanjing 201193, China. E-mail: jingzhao@nju.edu.cn
[b]School of Life Sciences, Nanjing University, Nanjing 210093, China
[c]Shenzhen Research Institute, Nanjing University, Shenzhen, 518000, China

†Electronic supplementary information (ESI) available. See DOI: 10.1039/c9nr08570j

‡These authors contributed equally to this work.

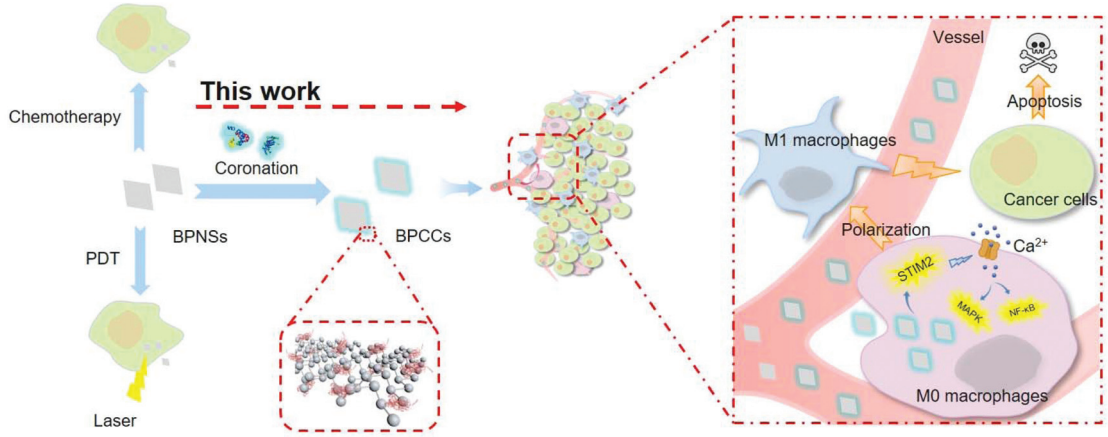

Scheme 1 Summary diagram of the regulation mediated by BP–corona complexes (BPCCs). BPNSs covered with a plasma protein corona could promote the activation and polarization of macrophages and enhance the anticancer ability of macrophages.

Results

Formation of the protein corona

BPNSs were obtained according to the protocols in previously published literature.[27] The mean lateral sizes of BPNSs were 128 nm by transmission electron microscopy (TEM) (Fig. 1a). After being covered with plasma proteins, the average height of BPNSs and BPCCs was 1.6 nm and 13.5 nm, which increased by 11.9 nm (Fig. 1b, d and S1†). The homogeneous distributions of C, N and P in the BPCCs were confirmed by EDS-elemental mapping (Fig. 1c), indicating the successful and dispersive coverage of BPNSs by plasma proteins. Furthermore, the average size of the BP nanomaterials also increased from 174 nm to 207 nm (Fig. 2a). To further analyse

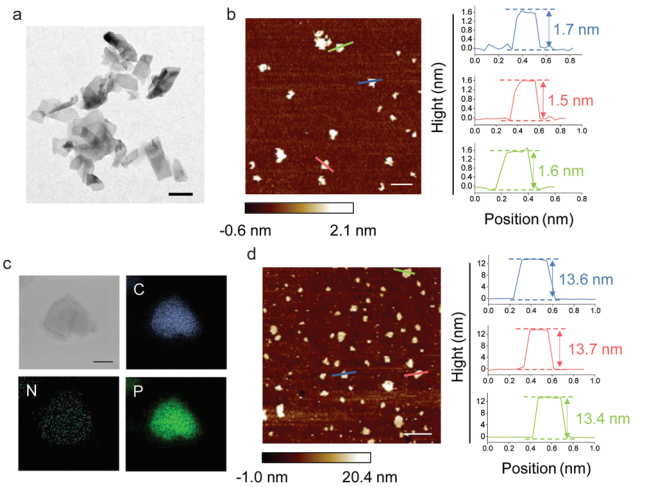

Fig. 1 Characterization of BPNSs and BPCCs. (a) TEM analysis of BPNSs. Scale bar: 200 nm. (b) AFM image of BPNSs. Scale bar: 500 nm. Right: corresponding height profiles along the coloured lines in the AFM image. (c) Area-elemental mappings of BPCCs. Scale bar: 100 nm. (d) AFM image of BPCCs. Scale bar: 500 nm. Right: corresponding height profiles along the coloured lines in the AFM image.

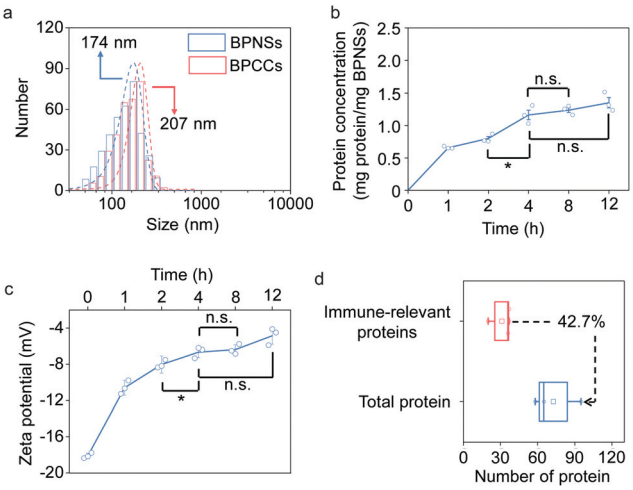

Fig. 2 Dynamic analysis and identification of corona formation. (a) Dynamic light scattering (DLS) analysis of BPNSs and BPCCs. (b) BCA protein assay of corona on BPCCs at different incubation times. (c) Zeta potential of BPCCs at different incubation times. (d) Analysis of the protein from BPCCs. All values are expressed as the mean ± SD of triplicates. Statistical significance was assessed by Student's *t* test. $*p < 0.05$, $**p < 0.01$.

corona formation, we detected the zeta potential and protein concentration of BPCCs (Fig. 2b and c). The zeta potential and protein concentration increased from −18.1 mV and 0 mg protein per mg BPNSs to −4.85 mV and 1.35 mg protein per mg BPNSs, respectively, and these effects were time-dependent. Specifically, after 8 h- and 12 h-incubation, the zeta potential and protein concentration were increased without reaching statistical significance, indicating that corona formation was balanced after 4 h of incubation. Compared to previous studies on rapid formation of corona in plasma,[13,28] BPNSs took 4 h to form a stable corona probably due to their unique surface chemistry.

Then, LC-MS/MS was used to determine the components of the corona (Fig. 2d). BPCCs contained on average 73 proteins,

31 of which were annotated as immune-relevant proteins according to gene ontology (GO) analysis (Fig. 2d and S2†). These results indicated that BPNSs mainly bind to immune-relevant proteins to form a corona and inspired us to further study the regulatory effect of BPCCs on immune cells.

Ca^{2+} influx responses in macrophages

Cell morphology has recently been highlighted as a robust integrated biomarker of cell function.[29,30] According to previous studies, macrophage polarization states demonstrate a hallmark morphology, including elongated projections for M2 cells and round and flattened morphologies for M1 cells.[31,32] After treatment with the BPCCs, we observed that the morphology of the treated macrophages was similar to that of IFN-γ/lipopolysaccharide (LPS)-induced M1 macrophages (Fig. S3†). To further determine whether BPCCs induce M1 macrophages, we examined the transcriptomes of BPCC-treated Raw264.7 cells for expression differences in M1- *versus* M2-type mRNAs by quantitative real-time polymerase chain reaction (RT-PCR). The results showed that compared with untreated macrophages, BPCC-exposed macrophages significantly upregulated the expression of M1-related markers (including tumour-necrosis factor (TNF)-α, iNOS, interleukin (IL)-12p40 and CD16). In addition, the mRNA levels of M2-related genes (including IL-10, CD206 and Arginase-I) decreased after treatment with the BPCCs (Fig. 3a). Besides, the M1 polarization was also determined by the expression of the surface marker CD80 using flow cytometry. As illustrated in Fig. 3b and Fig. S4,† BPCCs and LPS induced high levels of CD80 expression, while BPNSs showed parallel CD80 expression levels compared to untreated cells.

Next, we performed proteomic analysis of the total protein in the BPCC-treated and untreated macrophages to reveal the immunoregulation of macrophages by the BPCCs (Fig. 3c, S5 and S6†). The quantitative proteomic results showed 20 proteins with significant differences (Fig. 3d and Table S1†). Kyoto Encyclopedia of Genes and Genomes (KEGG) pathway analysis revealed that the calcium signalling pathway is the most likely pathway related to cell morphology (Fig. S7†). Stromal interaction molecule 2 (STIM2) showed the most differences among proteins in the calcium signalling pathway. As shown in Fig. 3e, the expression of STIM2 was increased 2.03-fold in the macrophages treated with the BPCCs. Precise LC-PRM/MS quantitative analysis was also applied to confirm the upregulation of STIM2 expression (Fig. 3f).

Store-operated Ca^{2+} entry (SOCE) is a ubiquitous Ca^{2+} entry pathway in different cells such as immune cells, and the stromal interaction molecule (STIM) proteins (including STIM1 and STIM2) and the Orai protein are the main proteins responsible for SOCE.[33–35] Increasing evidence has demonstrated that STIM2 plays a critical role in the regulation of Ca^{2+} influx and Ca^{2+}-dependent cell function at low stimulus intensities.[36,37] Moreover, the amplitude and duration of Ca^{2+} signals regulate gene expression, cytokine release and migration.[33] Thus, we further monitored the Ca^{2+} influx in macrophages based on the quantitative proteomic results. As

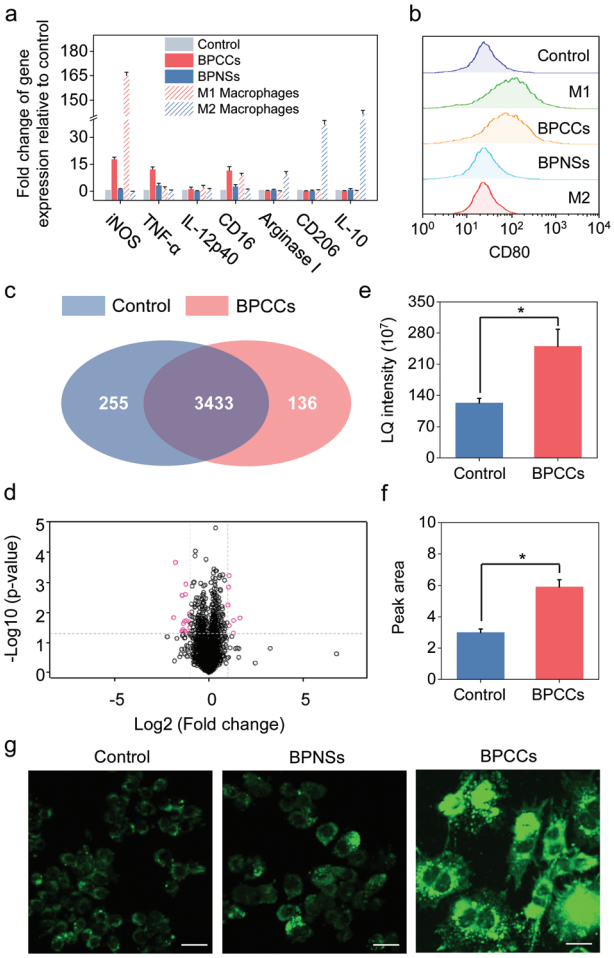

Fig. 3 Effect of BPCCs on Ca^{2+} influx and macrophage polarization. (a) Marker genes of M1 or M2 macrophages were measured in Raw264.7 cells with or without nanomaterial treatment by quantitative RT-PCR. (b) Surface CD80 expression in macrophages with or without nanomaterials analysed by flow cytometry. (c) Statistical analysis of the total number of proteins identified in Raw264.7 cells and BPCC-treated Raw264.7 cells by LC-MS/MS. (d) Volcano plot showing the *P* value (−log 10) *versus* the fold change in the protein ratio (log 2, BPCC-treated cells *versus* control cells). The dashed lines represent a 2-fold difference in abundance and a *p* value <0.05. (e) Label-free quantification analysis of the expression of STIM2 proteins in untreated cells and BPCC-treated cells. (f) LC-PRM/MS quantitative analysis of the expression of STIM2 proteins in untreated cells and BPCC-treated cells. (g) Effects of BPNSs and BPCCs on the intracellular Ca^{2+} concentration. Scale bar: 20 μm. Statistical significance was assessed by Student's *t* test. $*p < 0.05$, $**p < 0.01$.

shown in Fig. 3g and S8,† the mean fluorescence intensity (MFI) of Fluo-4 AM was 116.67, 141.29 and 402.39 in untreated cells, BPNS-treated cells and BPCC-treated cells, respectively, suggesting that the intracellular calcium concentration increased after treatment with the BPCCs. Furthermore, we eliminated Ca^{2+} in the culture medium to confirm that the increase in the Ca^{2+} concentration in the cytoplasm was associated with extracellular Ca^{2+} influx (Fig. S9 and S10†). The Ca^{2+} concentration barely changed in the BPNS/BPCC-treated cells in the Ca^{2+}-free culture medium compared with the treated

cells in the normal culture medium (Ca^{2+}-containing culture medium). Moreover, we tested the effect of BPCC-induced Ca^{2+} influx on macrophage polarization. A lack of Ca^{2+} in the culture medium resulted in the loss of the BPCCs' ability to induce M1 macrophages (Fig. S11†).

Ca^{2+} influx activated p38 and NF-κB

To further explore the interaction between BPCCs and STIM2, we first carefully examined the functions of all proteins on BPCCs (Table S2†). We discovered that the most abundant protein on BPCCs was myosin, a well-recognized calmodulin (CAM)-binding protein.[38–40] It is known that CAM could further bind and activate STIM2 to facilitate Ca^{2+} influx.[41–43] Therefore, we hypothesized that the interaction between BPCCs and STIM2 was mediated by CAM (Fig. 4a). The binding ability of CAM to BPCCs was evaluated in macrophage lysates to simulate the macrophage environment. As shown in Fig. 4b, BPCCs could interact with CAM through myosin. To determine whether CAM is involved in BPCC-mediated Ca^{2+} influx, calmidazolium chloride was used to block CAM. When macrophages were pre-treated with calmidazolium chloride, BPCC-induced Ca^{2+} influx was inhibited (Fig. 4c and d), and

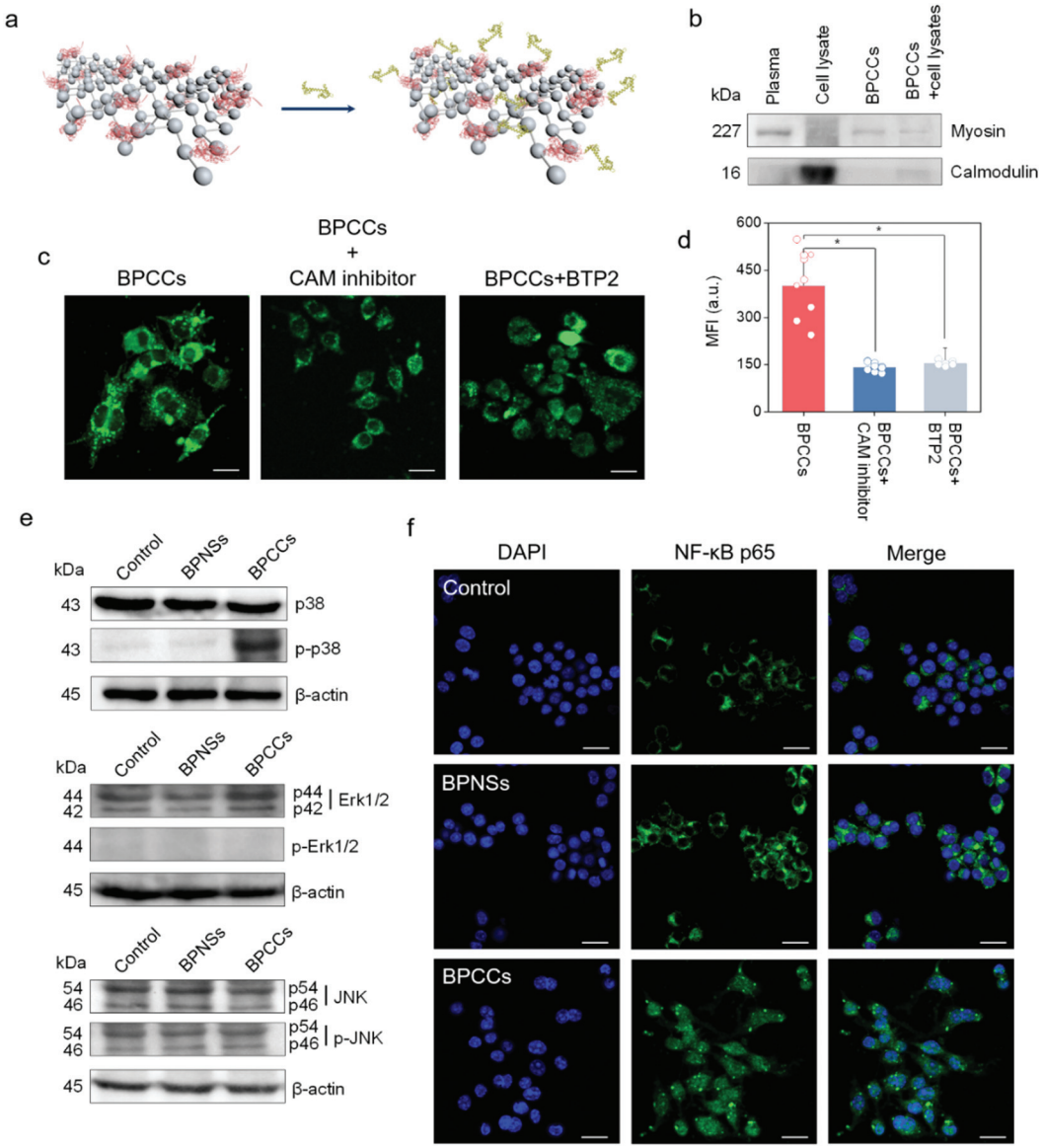

Fig. 4 Mechanistic insight into BPCC-induced macrophage polarization. (a) Diagram showing the adsorption of CAM (yellow) on BPCCs through myosin (red). (b) Western blot analysis of myosin and CAM on BPCCs after incubation with macrophage lysates. (c) Cellular imaging of Ca^{2+} with Fluo-4 AM. Cells were pre-treated with the inhibitor and then incubated with BPCCs. Scale bar: 20 μm. (d) Quantitative analysis of the MFI of Fluo-4 AM from c. (e) The phosphorylation of p38, Erk1/2 and JNK in Raw264.7 cells treated with 15 μg ml^{-1} BPNSs or BPCCs analysed by western blot analysis. (f) NF-κBp65 levels in Raw264.7 cells treated with BPCCs or left untreated as determined by fluorescence microscopy. Green, NF-κB p65; blue, nucleus. Scale bar: 20 μm. All values are expressed as the mean ± SD of triplicates. Statistical significance was assessed by Student's *t* test. $*p < 0.05$, $**p < 0.01$.

the upregulation of M1-related genes in BPCC-induced macrophages was also inhibited (Fig. S12†). To study the interaction between BPCCs and STIM2 in macrophages, we obtained fluorescent BPCCs by adding serum albumin that was conjugated to rhodamine B isothiocyanate (SA-RBITC) to plasma. The addition of SA-RBITC did not change the component of BPCCs (Fig. S13†). As shown in Fig. S14,† the overlap of fluorescent BPCCs and STIM2 indicated that most BPCCs could interact with the STIM2 protein. An inhibitor of the STIM proteins, BTP2, was utilized to further confirm that the BPCC-induced Ca^{2+} influx was associated with STIM2 (Fig. 4c and d). When BTP2 was added to the medium, unchanged expression of marker genes was observed, confirming that BPCC-induced macrophage polarization was associated with STIM2 (Fig. S15†).

Next, we investigated the signalling pathway through which BPCCs induce M1 macrophages. Mitogen-activated protein kinase (MAPK) and nuclear factor-κB (NF-κB) are key regulators of proinflammatory factors, and these proteins are activated in IFN-γ/LPS-induced M1 macrophages.[44,45] Here, we used western blot analysis and immunofluorescence to analyse MAPK and NF-κB expression in BPCC-induced M1 macrophages. After analysing the three MAPK members JNK, p38 and Erk 1/2, we found that only p38 was significantly phosphorylated in the BPCC-treated Raw264.7 cells, implying that p38 might be involved in the BPCC-induced macrophage phenotype switch (Fig. 4e and S16†). Then, we analysed NF-κB p65 by assessing its nuclear translocation. According to the immunofluorescence results, the entry of NF-κB p65 into the nucleus occurred in Raw264.7 cells after treatment with BPCCs (Fig. 4f). However, the untreated cells and BPNS-treated cells had no NF-κB p65 expression in the nucleus. On the other hand, blocking p38 or NF-κB p65 with inhibitors (SB203580, an inhibitor of p38; JSH-23, an inhibitor of NF-κB p65) resulted in a loss of the effect of BPCCs on induced M1 macrophages (Fig. S17†). Taken together, these results revealed that BPCCs could interact with STIM2 through CAM adsorption and induce Ca^{2+} influx to promote M1 macrophage development by activating p38 MAPK and NF-κB p65.

Effects of BPCCs on cancer cells and macrophages *in vitro*

According to previous reports, nanomaterials, including silica nanoparticles (NPs), ferumoxytol, and titanium dioxide, can attract alveolar macrophages.[46–48] To study whether BPCCs can attract macrophages, we first investigated their chemotactic properties *in vitro*. Using a Transwell system with 3 μm-sized microporous membranes (macrophages are able to migrate through 3 μm pores),[46] we assessed the migration of Dil-labelled macrophages (Fig. 5a). As shown in Fig. 5b and c, cancer cells and the BPCCs could each attract macrophages, and the combination of the BPCCs and cancer cells led to an additive effect on the migration of macrophages.

Macrophages are important members of the immune system, and phagocytosis is one of the significant cellular functions of macrophages.[49] Based on the above results, we further determined the effect of BPCCs on phagocytosis in

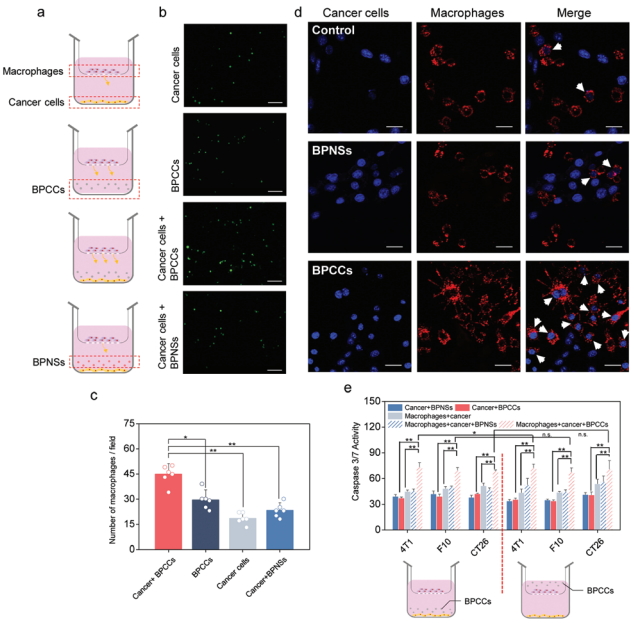

Fig. 5 BPCCs enhanced the anticancer effect of macrophages. (a) Diagram showing the macrophage-cancer cell co-culture model in Transwell plates (3 μm-sized microporous membrane that allows macrophage migration). (b) Migration of Dio-labelled macrophages (green) from the insert chamber to the bottom chamber. Macrophages were treated with 15 μg ml^{-1} BPNSs or BPCCs for 8 h, and the bottom chamber was analysed with fluorescence microscopy. Scale bar: 200 μm. (c) Statistical analysis of the number of macrophages that migrated to the bottom chamber. Macrophage cell counts were averaged from 5–10 fields of view using fluorescence microscopy. (d) Phagocytosis of DAPI-labelled 4 T1 cancer cells (blue) by Dil-labelled Raw264.7 cells (red) treated with BPCCs. Scale bar: 25 μm. (e) Caspase 3/7 activity of different cancer cell types in the co-culture model after the addition of 15 μg ml^{-1} nanomaterials to the insert or bottom chamber. All values are expressed as the mean ± SD of triplicates. Statistical significance was assessed by Student's *t* test. $*p < 0.05$, $**p < 0.01$.

macrophages (Fig. 5d). Cancer cells and macrophages were first labelled with different dyes and then co-cultured with Dil-labelled macrophages and DAPI-labelled cancer cells incubated with or without BPCCs. We found significantly more blue fluorescence overlapping with red fluorescence after incubation with the BPCCs, suggesting that the formation of a corona on BPNSs could promote the phagocytosis of cancer cells by macrophages. Then, we further studied the apoptosis of cancer cells in a co-culture model (Fig. 5e). We found markedly increased caspase 3/7 activity when different cancer cells were incubated with macrophages plus the BPCCs compared with when the cancer cells were incubated with either the macrophages or BPCCs alone. Moreover, the BPCCs could enhance the cytotoxicity of macrophages in a direct or indirect way.

To further determine whether BPCCs induce macrophage polarization, we isolated macrophages from the above-described co-culture model and analysed their transcriptomes through RT-PCR. As shown in Fig. 6a, compared with the untreated macrophages, the macrophages treated with the

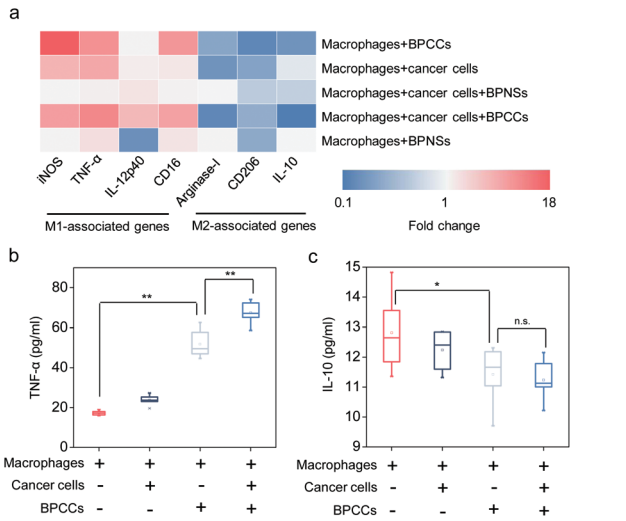

Fig. 6 BPCCs enhanced the anticancer effect of macrophages. (a) Gene expression levels of M1 and M2 macrophage markers measured in Raw264.7 cells treated with or without nanomaterials from the co-culture model by quantitative RT-PCR. (b–c) ELISA analysis of the concentrations of (b) TNF-α and (c) IL-10 in the culture medium. All values are expressed as the mean ± SD of triplicates. Statistical significance was assessed by Student's *t* test. **p* < 0.05, ***p* < 0.01.

BPCCs upregulated the expression of the M1-related molecules TNF-α, iNOS, IL-12p40 and CD16. In addition, the mRNA levels of the M2-related markers IL-10, CD206 and Arginase-I were significantly decreased after co-culturing macrophages with cancer cells and BPCCs. Then, we further verified the expression of IL-10 (M2-related marker) and TNF-α (M1-related marker) by enzyme-linked immunosorbent assay (ELISA). As shown in Fig. 6b and c, a 3.9-fold increase in TNF-α expression above the background level and a slight decrease in IL-10 expression were observed. These results suggested that BPCC-induced cancer cytotoxicity was coupled to M1 macrophage polarization.

Conclusions

Macrophage polarization is the pivotal process in macrophage-based immunotherapy, and a great number of nanomaterials have been explored to induce macrophage differentiation.[46,48,50] Most nanomaterials induce macrophage polarization in the blood circulation system, which means that interactions between nanomaterials and plasma proteins are unavoidable. However, knowledge of the relationships among nanomaterials, plasma proteins (corona proteins) and immune cells is lacking. This work reveals that 2D BP nanomaterials can adsorb plasma proteins to form BPCCs and that the accumulation of corona proteins on BPNSs exhibits specific regulation towards macrophages. Due to the opsonins in the corona, BPCCs were efficiently ingested by macrophages and interacted with the STIM2 protein to facilitate Ca^{2+} influx. Intriguingly, our findings suggest that BPCC-induced Ca^{2+} entry further promoted macrophage polarization, which is similar to a recent report showing that alteration of the metal ion concentration enabled the activation of T cells.[51] This finding reveals the critical role of the corona in immunotherapy for cancer and immune-related diseases. The current work may not only shed light on the important roles of BPCCs in the activation of macrophages but also open a new avenue for immune cell activation from the perspective of bio-nano interfaces.

Conflicts of interest

There are no conflicts to declare.

Acknowledgements

Financial support was provided by the National Natural Science Foundation of China (21622103, 21571098, 21671099 and 91753121) and the Shenzhen Basic Research Program (JCYJ20170413150538897), supported by the Fundamental Research Funds for the Central Universities (020514380139).

Notes and references

1 W. Chen, J. Ouyang, H. Liu, M. Chen, K. Zeng, J. Sheng, Z. Liu, Y. Han, L. Wang and J. Li, *Adv. Mater.*, 2016, **29**, 1603864–1603870.
2 L. Xi, W. Han, H. Shengxi, X. Fengnian and M. S. Dresselhaus, *Proc. Natl. Acad. Sci. U. S. A.*, 2015, **112**, 4523.
3 W. Hui, Y. Xianzhu, S. Wei, C. Shichuan, X. Junfeng, Z. Xiaodong, W. Jun and X. Yi, *J. Am. Chem. Soc.*, 2015, **137**, 11376–11382.
4 L. Chan, P. Gao, W. Zhou, C. Mei, Y. Huang, X.-F. Yu, P. K. Chu and T. Chen, *ACS Nano*, 2018, **12**, 12401–12415.
5 C. D. Walkey, J. B. Olsen, H. Guo, A. Emili and W. C. W. Chan, *J. Am. Chem. Soc.*, 2012, **134**, 2139–2147.
6 H. C. Fischer, L. Liu, K. S. Pang and W. C. W. Chan, *Adv. Funct. Mater.*, 2006, **16**, 1299–1305.
7 H. Liang, K. Huang, T. Su, Z. Li, S. Hu, P.-U. Dinh, E. A. Wrona, C. Shao, L. Qiao, A. C. Vandergriff, M. T. Hensley, J. Cores, T. Allen, H. Zhang, Q. Zeng, J. Xing, D. O. Freytes, D. Shen, Z. Yu and K. Cheng, *ACS Nano*, 2018, **12**, 6536–6544.
8 G. Qu, W. Liu, Y. Zhao, J. Gao, T. Xia, J. Shi, L. Hu, W. Zhou, J. Gao, H. Wang, Q. Luo, Q. Zhou, S. Liu, X.-F. Yu and G. Jiang, *Angew. Chem., Int. Ed.*, 2017, **56**, 14488–14493.
9 W. L. Murphy, T. C. McDevitt and A. J. Engler, *Nat. Mater.*, 2014, **13**, 547–557.
10 A. E. Nel, L. Mädler, D. Velegol, T. Xia, E. M. V. Hoek, P. Somasundaran, F. Klaessig, V. Castranova and M. Thompson, *Nat. Mater.*, 2009, **8**, 543–557.
11 P. C. Ke, S. Lin, W. J. Parak, T. P. Davis and F. Caruso, *ACS Nano*, 2017, **11**, 11773–11776.

12 H. Kong, K. Xia, N. Ren, Y. Cui, R. Liu, Q. Li, M. Lv, J. Shi, Q. Yan, Z. Cui, C. Fan, Y. Zhu and L. Wang, *Nanoscale*, 2018, **10**, 18055–18063.
13 D. Walczyk, F. B. Bombelli, M. P. Monopoli, I. Lynch and K. A. Dawson, *J. Am. Chem. Soc.*, 2010, **132**, 5761–5768.
14 M. P. Monopoli, D. Walczyk, A. Campbell, G. Elia, I. Lynch, F. Baldelli Bombelli and K. A. Dawson, *J. Am. Chem. Soc.*, 2011, **133**, 2525–2534.
15 M. P. Monopoli, C. Åberg, A. Salvati and K. A. Dawson, *Nat. Nanotechnol.*, 2012, **7**, 779–786.
16 D. Pozzi, V. Colapicchioni, G. Caracciolo, S. Piovesana, A. L. Capriotti, S. Palchetti, S. De Grossi, A. Riccioli, H. Amenitsch and A. Laganà, *Nanoscale*, 2014, **6**, 2782–2792.
17 A. Salvati, A. S. Pitek, M. P. Monopoli, K. Prapainop, F. B. Bombelli, D. R. Hristov, P. M. Kelly, C. Åberg, E. Mahon and K. A. Dawson, *Nat. Nanotechnol.*, 2013, **8**, 137–143.
18 B. Kang, P. Okwieka, S. Schöttler, S. Winzen, J. Langhanki, K. Mohr, T. Opatz, V. Mailänder, K. Landfester and F. R. Wurm, *Angew. Chem., Int. Ed.*, 2015, **54**, 7436–7440.
19 S. Schöttler, K. Landfester and V. Mailänder, *Angew. Chem., Int. Ed.*, 2016, **55**, 8806–8815.
20 C. Ge, J. Du, L. Zhao, L. Wang, Y. Liu, D. Li, Y. Yang, R. Zhou, Y. Zhao, Z. Chai and C. Chen, *Proc. Natl. Acad. Sci. U. S. A.*, 2011, **108**, 16968–16973.
21 S. Shahabi, L. Treccani, R. Dringen and K. Rezwan, *Nanoscale*, 2015, **7**, 16251–16265.
22 Z. Liu, X. Zhan, M. Yang, Q. Yang, X. Xu, F. Lan, Y. Wu and Z. Gu, *Nanoscale*, 2016, **8**, 7544–7555.
23 L. Wang, J. Li, J. Pan, X. Jiang, Y. Ji, Y. Li, Y. Qu, Y. Zhao, X. Wu and C. Chen, *J. Am. Chem. Soc.*, 2013, **135**, 17359–17368.
24 Z. Zhang, C. Wang, Y. Zha, W. Hu, Z. Gao, Y. Zang, J. Chen, J. Zhang and L. Dong, *ACS Nano*, 2015, **9**, 2405–2419.
25 Y. K. Lee, E. J. Choi, T. J. Webster, S. H. Kim and D. Khang, *Int. J. Nanomed.*, 2015, **10**, 97–113.
26 M. Hadjidemetriou, Z. Al-Ahmady, M. Mazza, R. F. Collins, K. Dawson and K. Kostarelos, *ACS Nano*, 2015, **9**, 8142–8156.
27 J. Mo, Q. Xie, W. Wei and J. Zhao, *Nat. Commun.*, 2018, **9**, 2480.
28 S. Tenzer, D. Docter, J. Kuharev, A. Musyanovych, V. Fetz, R. Hecht, F. Schlenk, D. Fischer, K. Kiouptsi, C. Reinhardt, K. Landfester, H. Schild, M. Maskos, S. K. Knauer and R. H. Stauber, *Nat. Nanotechnol.*, 2013, **8**, 772–781.
29 F. Y. McWhorter, T. Wang, P. Nguyen, T. Chung and W. F. Liu, *Proc. Natl. Acad. Sci. U. S. A.*, 2013, **110**, 17253–17258.
30 M. Okigaki, C. Davis, M. Falasca, S. Harroch, D. P. Felsenfeld, M. P. Sheetz and J. Schlessinger, *Proc. Natl. Acad. Sci. U. S. A.*, 2003, **100**, 10740–10745.
31 R. A. Marklein, J. Lam, M. Guvendiren, K. E. Sung and S. R. Bauer, *Trends Biotechnol.*, 2018, **36**, 105–118.
32 J. M. Phillip, P. H. Wu, D. M. Gilkes, W. Williams, S. Mcgovern, J. Daya, J. Chen, I. Aifuwa, J. S. H. Lee and F. Rong, *Nat. Biomed. Eng.*, 2017, **1**, 0093.
33 S. Feske, *Nat. Rev. Immunol.*, 2007, **7**, 690.
34 M. D. Cahalan, *Nat. Cell Biol.*, 2009, **11**, 669–677.
35 G. Barbet, M. Demion, I. C. Moura, N. Serafini, T. Léger, F. Vrtovsnik, R. C. Monteiro, R. Guinamard, J.-P. Kinet and P. Launay, *Nat. Immunol.*, 2008, **9**, 1148.
36 K. P. Subedi, H. L. Ong, G.-Y. Son, X. Liu and I. S. Ambudkar, *Cell Rep.*, 2018, **23**, 522–534.
37 O. Brandman, J. Liou, W. S. Park and T. Meyer, *Cell*, 2007, **131**, 1327–1339.
38 H. Nguyen and H. Higuchi, *Nat. Struct. Mol. Biol.*, 2005, **12**, 127–132.
39 C. Batters, D. Brack, H. Ellrich, B. Averbeck and C. Veigel, *Proc. Natl. Acad. Sci. U. S. A.*, 2016, **113**, E1162–E1169.
40 R. Stucchi, G. Plucińska, J. J. A. Hummel, E. E. Zahavi, I. Guerra San Juan, O. Klykov, R. A. Scheltema, A. F. M. Altelaar and C. C. Hoogenraad, *Cell Rep.*, 2018, **24**, 685–700.
41 C. B. Marshall, T. Nishikawa, M. Osawa, P. B. Stathopulos and M. Ikura, *Biochem. Biophys. Res. Commun.*, 2015, **460**, 5–21.
42 M. C. Bauer, D. O'Connell, D. J. Cahill and S. Linse, *Biochemistry*, 2008, **47**, 6089–6091.
43 R. Bhardwaj, H.-M. Müller, W. Nickel and M. Seedorf, *Biosci. Rep.*, 2013, **33**, e00077.
44 J. S. C. Arthur and S. C. Ley, *Nat. Rev. Immunol.*, 2013, **13**, 679.
45 E. Collignon, A. Canale, C. Al Wardi, M. Bizet, E. Calonne, S. Dedeurwaerder, S. Garaud, C. Naveaux, W. Barham, A. Wilson, S. Bouchat, P. Hubert, C. Van Lint, F. Yull, C. Sotiriou, K. Willard-Gallo, A. Noel and F. Fuks, *Sci. Adv.*, 2018, **4**, eaap7309.
46 S. Zanganeh, G. Hutter, R. Spitler, O. Lenkov, M. Mahmoudi, A. Shaw, J. S. Pajarinen, H. Nejadnik, S. Goodman, M. Moseley, L. M. Coussens and H. E. Daldrup-Link, *Nat. Nanotechnol.*, 2016, **11**, 986.
47 Y. Yang, Y. Lu, P. L. Abbaraju, J. Zhang, M. Zhang, G. Xiang and C. Yu, *Angew. Chem., Int. Ed.*, 2017, **56**, 8446–8450.
48 J. Wang, H.-J. Chen, T. Hang, Y. Yu, G. Liu, G. He, S. Xiao, B.-R. Yang, C. Yang, F. Liu, J. Tao, M. X. Wu and X. Xie, *Nat. Nanotechnol.*, 2018, **13**, 1078–1086.
49 H. Yuan, W. Jiang, C. A. von Roemeling, Y. Qie, X. Liu, Y. Chen, Y. Wang, R. E. Wharen, K. Yun, G. Bu, K. L. Knutson and B. Y. S. Kim, *Nat. Nanotechnol.*, 2017, **12**, 763.
50 Y. Min, K. C. Roche, S. Tian, M. J. Eblan, K. P. McKinnon, J. M. Caster, S. Chai, L. E. Herring, L. Zhang, T. Zhang, J. M. DeSimone, J. E. Tepper, B. G. Vincent, J. S. Serody and A. Z. Wang, *Nat. Nanotechnol.*, 2017, **12**, 877–882.
51 S. K. Vodnala, R. Eil, R. J. Kishton, M. Sukumar, T. N. Yamamoto, N.-H. Ha, P.-H. Lee, M. Shin, S. J. Patel, Z. Yu, D. C. Palmer, M. J. Kruhlak, X. Liu, J. W. Locasale, J. Huang, R. Roychoudhuri, T. Finkel, C. A. Klebanoff and N. P. Restifo, *Science*, 2019, **363**, eaau0135.